

Received:  
28 December 2017  
Revised:  
5 April 2018  
Accepted:  
25 June 2018

Cite as: Elias E. Elemike,  
Henry U. Nwankwo,  
Damian C. Onwudiwe.  
Synthesis and characterization  
of Schiff bases NBBA,  
MNBA and CNBA.  
Heliyon 4 (2018) e00670.  
doi: [10.1016/j.heliyon.2018.e00670](https://doi.org/10.1016/j.heliyon.2018.e00670)



# Synthesis and characterization of Schiff bases NBBA, MNBA and CNBA

Elias E. Elemike<sup>a,b,c</sup>, Henry U. Nwankwo<sup>a,b</sup>, Damian C. Onwudiwe<sup>a,b,\*</sup>

<sup>a</sup> Material Science Innovation and Modelling (MaSIM) Research Focus Area, Faculty of Natural and Agricultural Science, North-West University, Mafikeng Campus, Private Bag X2046, Mmabatho 2735, South Africa

<sup>b</sup> Department of Chemistry, School of Mathematics and Physical Sciences, Faculty of Natural and Agricultural Science, North-West University, Mafikeng Campus, Private Bag X2046, Mmabatho 2735, South Africa

<sup>c</sup> Department of Chemistry, College of Science, Federal University of Petroleum Resources, P.M.B 1221, Effurun, Delta State, Nigeria

\* Corresponding author.

E-mail address: [Damian.Onwudiwe@nwu.ac.za](mailto:Damian.Onwudiwe@nwu.ac.za) (D.C. Onwudiwe).

## Abstract

Three Schiff base compounds,  $N^1, N^2$ -bis(3-nitrobenzylidene)phenylene diamine (NBBA), 2-methyl- $N$ -(3-nitrobenzylidene)aniline (MNBA) and  $N$ -(2-chlorobenzylidene)-4-nitroaniline (CBNA) were synthesized, characterised and applied for the first time as potential mild steel (MS) corrosion inhibitors in 1 M HCl at 30 °C. Fourier transform infra-red (FTIR),  $^1\text{H}$ ,  $^{13}\text{C}$  Nuclear magnetic resonance (NMR) and Mass spectrometry (MS) were used for the characterisation of the compounds. The electrochemical studies and evaluation of corrosion inhibition potency were achieved using potentiodynamic polarization (PDP) and electrochemical impedance spectroscopy (EIS) techniques. Density functional theory (DFT) calculations were further employed to describe the electronic distribution on the molecules and potential sites that aided corrosion inhibition. The results of the employed characterisation techniques confirmed the proposed structures of the compounds with the MS revealing the exact molecular mass of the compounds. Electrochemical results showed that the trend in inhibition efficiency of the three compounds was in the order: MNBA > NBBA > CBNA. MNBA recorded the highest inhibition efficiency at 100 ppm. Corrosion kinetics of the set of inhibitors was found to prefer the Langmuir

adsorption isotherm with both physisorption and chemisorption mechanisms as revealed by  $\Delta G$  values. In an effort to develop efficient corrosion inhibitors with non-toxic effect, low cost and multiple adsorption centres, these Schiff bases are presented.

Keywords: Chemistry, Electrochemistry, Materials science

## 1. Introduction

Schiff base ligands are important class of organic molecules that could be referred to as seen as 'privileged ligands due to their simple and easy preparation route from the reaction of aldehydes or ketones with amines'. They have high tendency of forming coordination compounds with metals of varying oxidation states [1, 2, 3, 4, 5, 6]. Most Schiff base compounds have been prepared by reaction of a carbonyl compound, especially an aldehyde, and a primary amine with the elimination of a water molecule [7]. When using ketones, they tend to form imines at extended time under high temperature conditions which makes it uncommon among the substrates of Schiff base. [7]. When ketones are used, the compounds with aromatic groups are less reactive and would require harsh conditions compared to the aliphatic ones [8]. The chemistry of the synthesis of Schiff bases has shown that when organic acids such as glacial acetic acid are added and water removed during the reaction, the yields tends to increase.

The stability, electroactive, thermochromic and photochromic nature of Schiff base compounds has made them excellent intermediates for various applications [9, 10, 11]. The flexibility of the azomethine group associated with this group of compounds, which enables attachment and extension of  $\pi$  donating groups, has interestingly widened the scope of Schiff bases, thereby attracting the interest of corrosion chemists for their possible use in metal surface protection [12]. Schiff bases have been used as corrosion inhibitors because they can easily be synthesized, contain aromatic rings that offer electron cloud, and can also incorporate some electronegative atoms as substituents which could determine their overall potency and helps in technological advancement of better corrosion inhibitors [13]. The C=N group, planarity of  $\pi$ -bonding orbitals and electrons from the attached electronegative atoms afford them the great opportunity of being adsorbed on the metal surfaces [14].

There is an increasing desire to combat corrosion of metals as recent survey reported worldwide cost of corrosion control to the estimated sum of US \$2.5 trillion [15, 16]. It is therefore a challenge to material scientists to develop high yield, cost effective, low toxic and efficient corrosion inhibitors that can be employed as additives in paint production and organic coating. A survey of the literature showed that Schiff base compounds have been reported as efficient corrosion inhibitors for metals in acidic media [17, 18, 19].

In this report, three Schiff base compounds with structural similarities, containing nitro groups and aromatic rings, were synthesised and their inhibition activities for mild steel in acidic medium was studied by electrochemical methods.

This paper is a continuation of our earlier works on Schiff bases, which focus on substituent effects of Schiff bases for potential application as mild steel corrosion inhibitors [20, 21, 22]. Theoretical calculations using DFT models were also utilised to explain the basic sites of electron transfer involved in the inhibition process.

## 2. Experimental

### 2.1. Materials

1,2-phenylenediamine, 3-nitrobenzaldehyde, 2-methylaniline, 4-nitroaniline, 2-chlorobenzaldehyde were used as received from the supplier (Merck).

### 2.2. Spectral and instrumental measurements

FTIR measurements of the compounds were carried out using a Bruker alpha-P FTIR spectrophotometer in the wavenumber range of 400–4000  $\text{cm}^{-1}$ . The  $^1\text{H}$  and  $^{13}\text{C}$  NMR analyses were carried out using 600 MHz Bruker Avance III NMR spectrometers at room temperature and DMSO was used as solvent.

Electrochemical characterisation techniques such as potentiodynamic polarization (PDP) and electrochemical impedance spectroscopy (EIS) were carried out using Autolab PGSTAT 302N obtained from Metrohm. The make-up of the instrument includes a three electrode system; mild steel, platinum rod and Ag/AgCl with 3 M KCl serving as working, counter and reference electrodes respectively. Surface characterisations of the materials combined with simultaneous elemental characterisation were done using Quanta FEG 250 Environmental scanning electron microscope (ESEM) under an acceleration voltage of 15 kV in high vacuum.

### 2.3. Synthesis of compounds: $N^1, N^2$ -bis(3-nitrobenzylidene) phenylenediamine (NBBA), (Z)-2-methyl-N-(3-nitrobenzylidene) aniline (MNBA) and (Z)-N-(2-chlorobenzylidene)-4-nitroaniline (CBNA) Schiff bases

In the first synthesis, equimolar concentration of benzene-1,2-diamine (5 mmol) and 3-nitrobenzaldehyde (10 mmol) were refluxed in 25 mL absolute ethanol. This was followed by the addition of 2–3 drops of glacial acetic acid and the mixture was allowed to react for 2 h. The resulting product obtained was rinsed with warm ethanol to give yellowish precipitate (NBBA). Similar synthetic procedures were followed for the synthesis of MNBA by reacting equimolar quantities of 1.70 mL of 2-methylaniline and 0.15 g of 3-nitrobenzaldehyde, and also for CBNA by reacting

1.38 g of 4-nitroaniline and 1.40 mL 2-chlorobenzaldehyde, under the same conditions.

**NBBA** Yield: 16.28%. Selected FTIR ( $\text{cm}^{-1}$ ): 3065  $\nu(\text{H}-\text{C}=\text{C})$ , 1678, 1623  $\nu(\text{C}=\text{C})$  1608  $\nu(\text{C}=\text{N})$ , 1524s  $\nu(\text{C}=\text{C})$ , 1347, 1188 (Ar-NO<sub>2</sub>), 1092, 967,751 (m-benzene ring).

<sup>1</sup>H NMR: (DMSO,  $\delta$  ppm): 7.23, 7.36, 7.43, 7.65, 8.22, 8.26 (m, C<sub>6</sub>H<sub>4</sub>), 8.85 (s, N=CH).

<sup>13</sup>C NMR (DMSO,  $\delta$  ppm): 116.2, 123.9, 125.9, 126.7, 129.7, 133.7, 135.3, 149.6, 150.9 (C<sub>6</sub>H<sub>4</sub>), 163.9 (HC=N). MS (ESI)  $m/z = \text{C}_{20}\text{H}_{14}\text{N}_4\text{O}_4$ . Calcd, 374.29; Found [M+H]<sup>+</sup> 375.10 (100%). Anal. cal for C<sub>20</sub>H<sub>14</sub>N<sub>4</sub>O<sub>4</sub>: C, 64.17; H, 3.77; N, 14.97; Found: C, 64.01; H, 3.54; N,14.60%.

**MNBA** Yield: 72.41%. Selected FTIR ( $\text{cm}^{-1}$ ): 3071  $\nu(\text{H}-\text{C}=\text{C})$ , 2957, 2911,  $\nu(\text{H}-\text{C}-)$ , 1624  $\nu(\text{C}=\text{N})$ , 1524 $\nu(\text{C}=\text{C})$ , 1344, 1183 (Ar-NO<sub>2</sub>), 1073, 977, 777, 755 (p-benzene ring).

<sup>1</sup>H NMR: (DMSO,  $\delta$  ppm): 2.30, 2.49 (d, CH<sub>3</sub>), 7.06, 7.14, 7.16, 7.24, 7.78, 7.81, 8.33, 8.36 (m, C<sub>6</sub>H<sub>4</sub>), 8.71 (s, N=CH). <sup>13</sup>C NMR (DMSO,  $\delta$  ppm): 17.6 (CH<sub>3</sub>), 117.6, 122.9, 125.7, 126.5, 126.9, 130.4, 131.8, 134.7, 137.8, 149.3, 149.7, 158.1 (C<sub>6</sub>H<sub>4</sub>), 189.9 (HC=N). MS (ESI)  $m/z = \text{C}_{14}\text{H}_{12}\text{N}_2\text{O}_2$ . Calcd 240.45; Found [M+H]<sup>+</sup> 241.09 (100%). Anal. cal for C<sub>14</sub>H<sub>12</sub>N<sub>2</sub>O<sub>2</sub>: C, 69.99; H, 5.03; N, 11.66; Found: C, 69.54; H, 5.35; N,11.30%.

**CBNA** Yield: 87.06%. Selected FTIR ( $\text{cm}^{-1}$ ): 3105, 3073 (H-C=C), 1600,  $\nu(\text{C}=\text{N})$ , 1509,  $\nu(\text{C}=\text{C})$ , 1337, 1193 (Ar-NO<sub>2</sub>), 1049, 859,755 (o, p-benzene ring). <sup>1</sup>H NMR: (DMSO,  $\delta$  ppm): 2.49 (s, CH-Cl), 6.57, 6.70, 7.41, 7.53, 7.69, 8.02 (m, C<sub>6</sub>H<sub>4</sub>), 10.32 (s, N=CH); <sup>13</sup>C NMR (DMSO,  $\delta$  ppm): 117.5, 126.3, 126.5,128.4, 129.6, 130.6, 132.2,133.1, 135.7, 136.4,152.9, 155.8 (C<sub>6</sub>H<sub>4</sub>), 168.9 (HC=N).

MS (ESI)  $m/z = \text{C}_{13}\text{H}_9\text{N}_2\text{O}_2$ . Calcd. 260.68; Found [M+H]<sup>+</sup> 261.04 (100%). Anal. cal for C<sub>13</sub>H<sub>9</sub>N<sub>2</sub>O<sub>2</sub>: C, 59.90; H, 3.48; N, 10.75%; Found: C, 59.74; H, 3.85; N, 10.35%.

## 2.4. Material preparation for corrosion studies

Mild steel (MS) coupons with composition of 0.17% C, 0.46% Si, 0.017% S, 0.019% P, and the rest Fe, were used for corrosion studies. The MS coupons used as working electrode (WE) were cut into 1 cm × 1 cm, and were embedded in a Teflon holder using epoxy resin, exposing only a surface area of 1 cm<sup>2</sup>. Before commencement of electrochemical test, MS surface was refined on Struers MD Piano<sup>TM</sup> 220. The shiny surface was enhanced by grinding with finer SiC papers. The shiny coupons were each washed in a sonicating acetone and ethanol bath for 40 min. The air-dried shiny

coupons were used for the corrosion tests. The 1 M HCl solution was prepared by diluting the analytical grade (32%) with distilled water. The inhibitor concentrations: 10, 40, 60 and 100 ppm were prepared in mixture of acetone and distilled water, followed by sonication for 1 h.

## 2.5. Theoretical modelling and optimization studies

The molecular structure of the ligand molecule was optimized by the DFT method with a hybrid functional B3LYP (Becke's three parameter Hybrid Functional using the LYP Correlation Function) at 6-31G+ (d, p) basis set [23, 24]. Complete geometry optimizations of the neutral compounds under study were carried out both *in vacuo* and in water phases by using Gaussian 09 program package [25, 26, 27, 28]. In addition, Frontier molecular orbitals (FMO) and thermodynamic properties were performed with the same level of theory. The same level of theory was further employed to gauge the chemical activities of the compounds in water using the polarizable continuum model [29]. Furthermore, complete geometry optimizations and FMO descriptors were in addition recorded for protonated form of inhibitor molecules in order to ascertain their true behaviour in 1 M HCl solution. The inhibitors were doubly-protonated at N- and O-heteroatoms. Most of the parameters were obtained from FMO according to the following Equations (1), (2), (3), (4), and (5) [22, 29]:

$$\Delta E = E_{LUMO} - E_{HOMO} \quad (1)$$

$$\eta = -\frac{1}{2}(E_{HOMO} - E_{LUMO}) \quad (2)$$

$$\sigma = \frac{1}{\eta} = -\left(\frac{2}{E_{HOMO} - E_{LUMO}}\right) \quad (3)$$

$$\mu = \frac{1}{2}(E_{HOMO} + E_{LUMO}) \quad (4)$$

$$\omega = \frac{\mu^2}{2\eta} \quad (5)$$

where  $\Delta E$  is energy band gap,  $\eta$  is chemical hardness,  $\sigma$  is chemical softness,  $\mu$  is chemical potential and  $\omega$  is electrophilicity index.

## 2.6. Electrochemical measurements

Before commencement of electrochemical tests, the system was allowed to attain the steady open circuit potential (OCP). The potential scan was conducted for 30 min in the aggressive solutions without and with various concentrations of inhibitors. The PDP studies were conducted after 30 min of MS immersion in the aggressive

solutions by sweeping the potential from  $-0.250$  up to  $+0.250$  mV (vs Ag/AgCl, 3 M KCl) at the scan rate of  $5 \text{ mV s}^{-1}$ . During the potentiodynamic scan conducted at  $5 \text{ mV s}^{-1}$ , a steady state was reached. In a bid to ensure adequate description of the electrochemical corrosion system, different scan rate values have been used and reported elsewhere [14, 29]. The EIS measurements were performed at the OCP by analysing the frequency feedback of the system in the range of 10 mHz–100 kHz at 10 mV amplitude.

The inhibition efficiency due to potentiodynamic polarization ( $\%IE_{PDP}$ ) measurements was calculated from the  $i_{corr}$  using the formula as shown in Equation (6) [22, 29]:

$$IE_{PDP} = 100 \left( 1 - \frac{i_{corr}}{i_{corr}^0} \right) \quad (6)$$

where  $i_{corr}^0$  and  $i_{corr}$  are corrosion current densities in the absence and presence of inhibitors respectively.

Similarly, the corrosion inhibition efficiency due to impedance measurements was evaluated from  $R_{ct}$  values using the formula shown in Equation (7) [22, 29]:

$$IE_{EIS} = 100 \left( \frac{R_{ct} - R_{ct}^0}{R_{ct}} \right) \quad (7)$$

where  $R_{ct}$  and  $R_{ct}^0$  are the charge transfer resistance in the presence and absence of inhibitor respectively. The experimentally generated impedance spectra were fitted using Nova 1.10.1.9 program [20, 21, 22, 29].

### 3. Results & discussion

#### 3.1. Synthesis of some nitro substituted Schiff base compounds

The three nitro substituted Schiff bases were synthesized from primary amines viz; phenylenediamine, 2-methylaniline, 4-nitroaniline and corresponding aromatic aldehydes; 3-nitrobenzaldehyde and 2-chlorobenzaldehyde in ethanol solution. All the obtained Schiff bases are yellowish in colour and soluble in ethanol, dimethyl formamide, chloroform, and dichloromethane, but sparingly soluble in methanol. The compounds are very stable at room temperature, and the synthetic pathways are shown in Fig. 1a–c.

#### 3.2. FTIR spectroscopy

There were interesting vibrations that characterized the synthesized compounds in the infrared spectra. In the spectrum of NBBA, stretching vibrations due to  $=C-H$  of the aromatic ring was observed around  $3065 \text{ cm}^{-1}$ . The strong bands

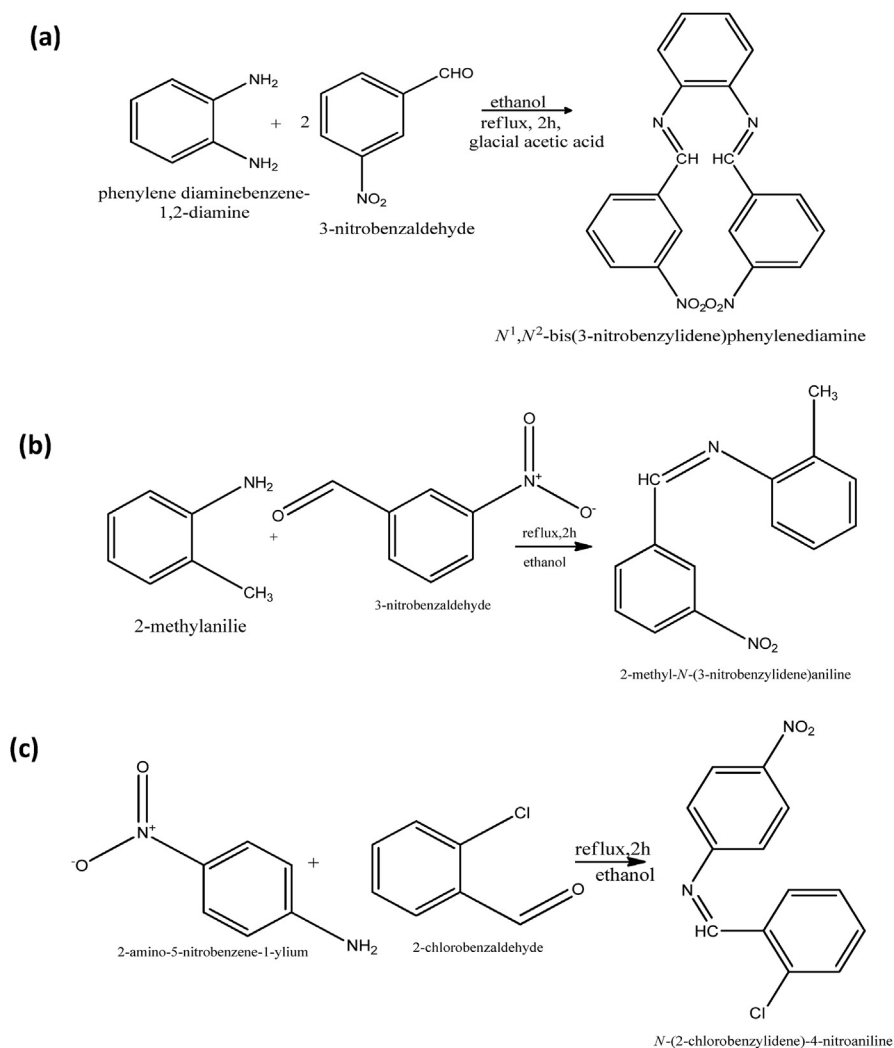


**Fig. 1.** Synthetic reaction pathway for the formation of (a)  $N^1,N^2$ -bis(3-nitrobenzylidene)phenylene diamine, (b) 2-methyl- $N$ -(3-nitrobenzylidene)aniline, and (c)  $N$ -(2-chlorobenzylidene)-4-nitroaniline.

which appeared between  $1678$  and  $1524\text{ cm}^{-1}$  could be ascribed to the  $\text{C}=\text{C}$  bending and  $\text{C}=\text{N}$  stretching vibrations respectively, attached to aromatic system. The bands at  $1347\text{ cm}^{-1}$  may be due to the  $\text{C}-\text{NO}_2$  bonds [30]. The bands at  $1092\text{ cm}^{-1}$  could be due to in-plane and out of plane deformation of  $\text{C}-\text{H}$ . In the spectrum of MNBA, the band at  $3071\text{ cm}^{-1}$  was due to the  $\text{C}-\text{H}$  of a  $\text{sp}^2$  hybridized carbon, whereas vibrations around  $2957\text{--}2879\text{ cm}^{-1}$  were assigned to the  $\text{C}-\text{H}$  bands attached to  $\text{sp}^3$  carbon. The  $\text{C}=\text{N}$  peak, in this case, appeared at  $1624\text{ cm}^{-1}$  and the band at  $1524\text{ cm}^{-1}$  may be due to  $\text{C}=\text{C}$  vibrations [20]. The spectrum of CBNA showed similar vibrational bands as observed in the other compounds, with the  $\text{C}=\text{N}$  group appearing as a very sharp band around  $1600\text{ cm}^{-1}$  and other sharp peaks at  $1509$ ,  $1337$  are characteristic of attachments to  $\text{C}=\text{C}$  bonds of the aromatic rings [31].

### 3.3. $^1\text{H}$ and $^{13}\text{C}$ NMR studies

Similar chemical shifts were obtained in the spectra of the three compounds as they have common backbones. In the spectrum of NBBA, the aromatic protons appeared between 7.23 and 8.26 ppm, and the HC=N peak was observed at 8.85 ppm. The  $^{13}\text{C}$ NMR spectrum showed aromatic carbon peaks between 116.1 and 150.9 ppm and the carbon of the HC=N moiety resonated at 163.9 ppm. The spectrum of MNBA showed a peak at 2.3 ppm, which could be ascribed to the protons of the methyl substituent, and the aromatic protons resonated between 7.1 and 8.4 ppm. The azomethine proton appeared at 8.7 ppm. The  $^{13}\text{C}$ NMR spectrum showed a peak at 17.6 ppm which is attributed to the methyl carbon and the carbons of the aromatic group appeared as approximately 12 peaks between 117.6 – 189.9 ppm. The peak due to the carbon of the C=N was recorded at 189.9 ppm. The  $^1\text{H}$ NMR of the chloro-containing Schiff base, CBNA, have chemical shifts attributed to aromatic protons between 6.57 and 8.02 ppm, and the proton of HC=N appeared at 10.32 ppm owing to the electron withdrawing effect of the chloro substituent which exerts some deshielding effect on the electrons around the molecule, thereby resulting to downfield shift. The  $^{13}\text{C}$ NMR spectrum showed the aromatic carbon peaks between 117.4 and 155.7 ppm while the resonant frequency of the carbon of the C=N was observed at 168.9 ppm.

### 3.4. Mass spectroscopy

The mass spectra of the three compounds are shown in Figs. 2, 3, and 4. The molecular ion peaks appeared at 375.10, 241.09 and 261.04 for NBBA, MNBA and CBNA respectively, and they reflect the molecular weight of the proposed structures. The  $\text{M}^+$  peaks are also the base peaks from the spectra which show the high stability of the prepared compounds [31].

### 3.5. Electrochemical experiments

#### 3.5.1. OCP and PDP studies

The potential was scanned over a period of 1800 s following the immersion of MS in the test solution. The OCP vs. time profile is shown in Fig. 5. The profile can be seen

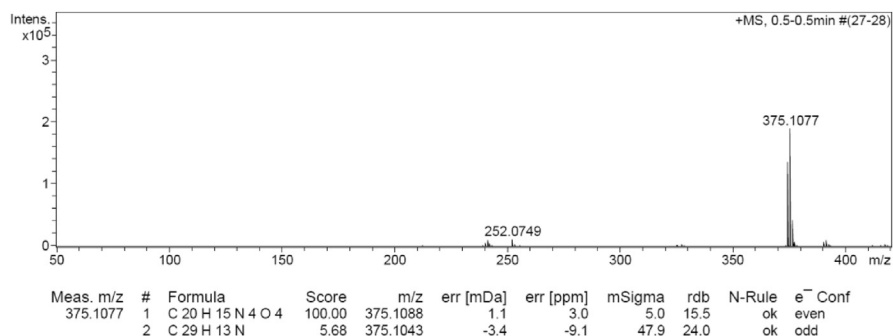
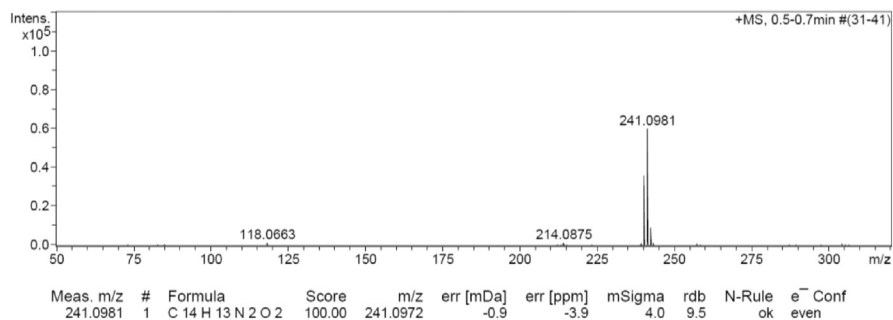
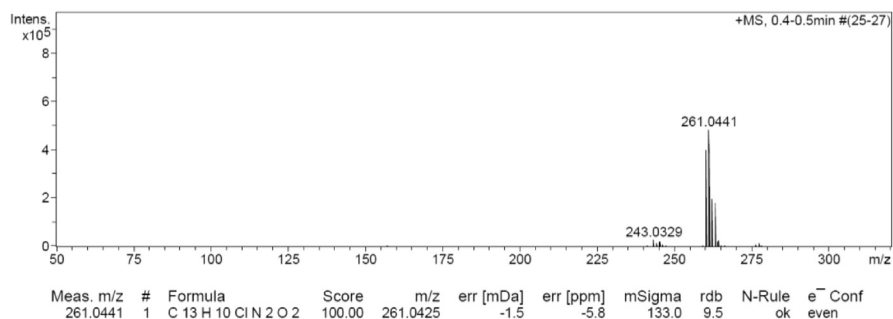


Fig. 2. Mass spectrograph of the NBBA.



**Fig. 3.** Mass spectrograph of the MNBA.



**Fig. 4.** Mass spectrograph of the CBNA.

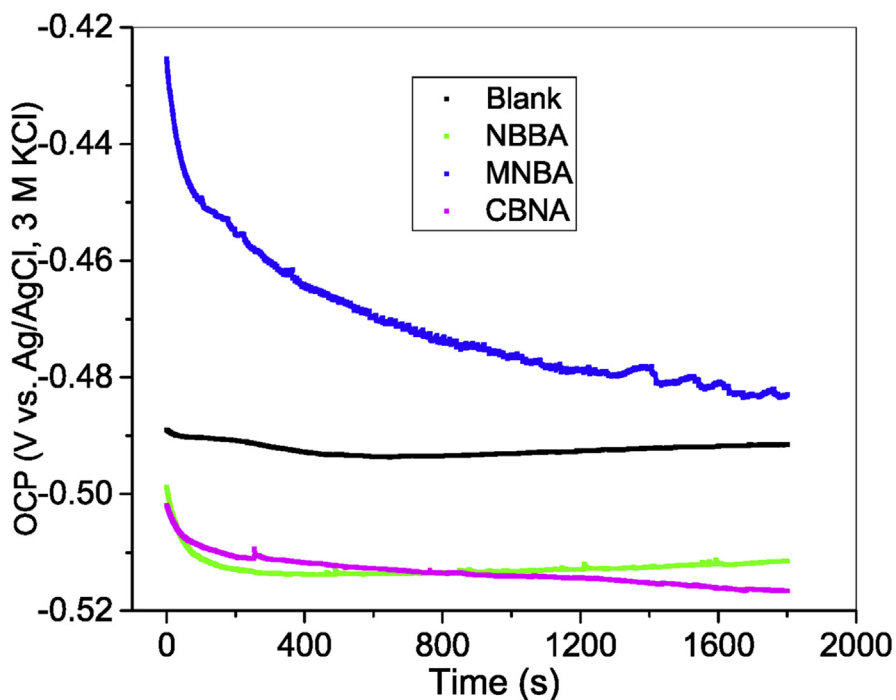


**Fig. 5.** Representative OCP scan for MS immersed in aggressive solutions in the absence and presence of 10 ppm of inhibitors.

to be stable at approximately 1400 s of immersion in all the tested solutions. This confirmed that the waiting period of 1800 s employed for OCP stabilization is therefore adequate for the study.

Fig. 6 shows the potentiodynamic anodic and cathodic polarization curves for MS in 1 M HCl solution, in the absence and presence of varying concentrations of NBBA, MNBA and CBNA at 30 °C. The relevant kinetic parameters, including anodic Tafel slope ( $\beta_a$ ), cathodic Tafel slope ( $\beta_c$ ), corrosion potential ( $-E_{corr}$ ), corrosion current density ( $i_{corr}$ ) and inhibition efficiency ( $IE_{PDP}\%$ ) are presented in Table 1. It can be observed in Fig. 6 that cathodic curves recorded a significant lower current density in contrast to a pronounced reduction observed for anodic curves for the three inhibitors. The occurrence of such phenomenon suggests that in the presence of the Schiff bases, there was a reduction in both cathodic and anodic current densities, particularly in the cathodic branch [21, 32]. The apparent negative shift in the corrosion potentials and the significant variations in both the cathodic and anodic current densities recorded for the compounds are presented in Table 1, and suggest that these compounds act as mixed-type inhibitors. The change in  $\beta_c$  with change in inhibitor concentrations suggests the influence of the inhibiting molecules on the mechanisms of the cathodic activity. In addition, the change in  $\beta_a$  connotes the agglomeration of

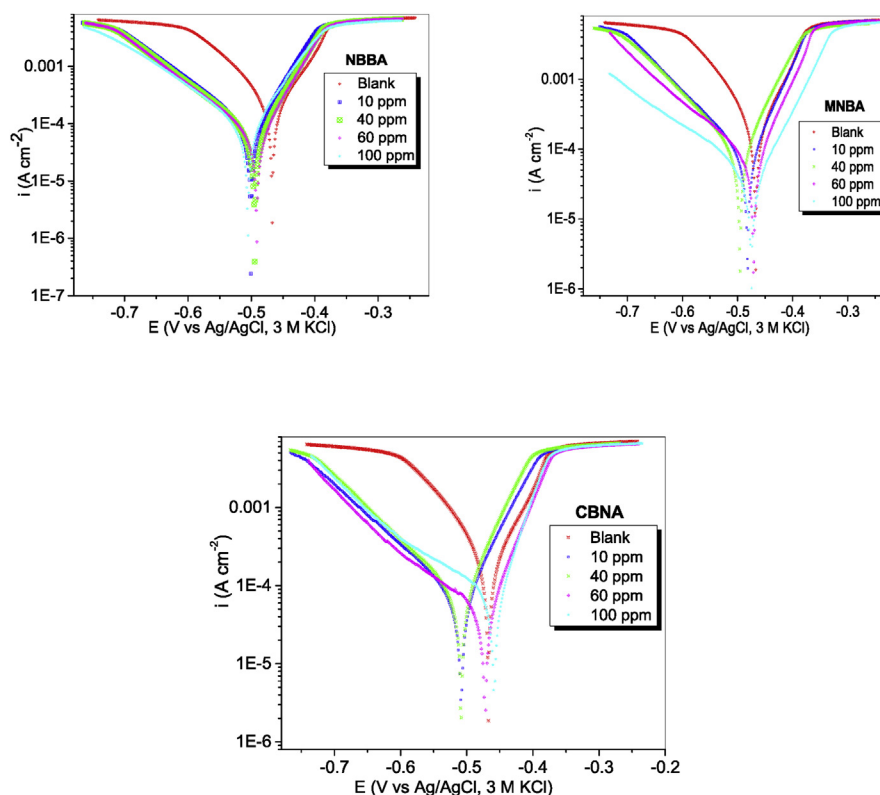


Fig. 6. Polarization curves of MS in 1 M HCl (blank) in the absence and presence of NBBA, MNBA and CBNA at the following concentrations: 10, 40, 60 and 100 ppm.

**Table 1.** Kinetic parameters from Tafel plots for MS in 1 M HCl in the absence and presence of NBBA, MNBA and CBNA at various concentrations.

Inhibitor	Conc (ppm)	$\beta_a$ (mV/dec)	$\beta_c$ (mV/dec)	$-E_{\text{corr}}$ (mV)	$i_{\text{corr}}$ ( $\mu\text{A cm}^{-2}$ )	$\eta\%$
Blank	—	98.93	72.08	452.72	236	—
NBBA	10	120.29	61.61	500.60	87	63
	40	120.04	59.32	494.79	68	71
	60	51.68	101.59	491.57	47	80
	100	50.64	84.93	505.49	40	82
MNBA	10	119.72	60.06	482.02	71	70
	40	62.85	95.78	495.65	68	71
	60	128.95	52.60	470.90	42	82
	100	150.41	64.46	475.48	25	89
CBNA	10	144.50	71.92	508.21	93	60
	40	55.45	125.58	508.58	70	70
	60	179.74	56.72	472.24	68	71
	100	152.16	45.8	458.34	62	74

chloride ions or MS-Schiff base species arising from redox activities on the selected sites on the MS surface [33].

Furthermore, an increase in inhibitor concentration with inhibition efficiency was followed by a decline in corrosion current densities.

### 3.5.2. EIS studies

An impedance measurement has an edge over potentiodynamic polarization measurement in unravelling both the resistive and capacitive behaviours at interfaces. The Nyquist plots of plain and varying concentrations of inhibitor containing solutions of NBBA, MNBA and CBNA in 1 M HCl are presented in Fig. 7. The plots are uniquely marked by a single capacitive loop in the form of depressed semicircles whose centre is below the x-axis. Frequency dispersion due to surface roughness of the working electrode surface has been blamed for such digression from ideal circular shape [21, 34, 35]. A further inspection of Fig. 7 reveals that the impedance of an inhibited substrate adjudged by the diameter of Nyquist plots was observed to increase relative to the concentration of inhibitors in corrosive environments. This therefore proves that inhibitors successfully formed protective film on MS surface [34, 35].

The single maxima which correspond to one time-constant observed for the Bode phase angle plots of Fig. 8 indicate that the entire corrosion process involved a single charge transfer mechanism. The impedance parameters, including  $R_{ct}$ ,  $Y_0$  and  $n$  were computed by fitting the EIS data using the equivalent circuit of Fig. 8 and are presented in Table 2 together with the percentage inhibition efficiency ( $IE_{EIS}\%$ ). The representative results of the fittings are given in Fig. 9, supporting the chosen equivalent circuit. Charge transfer resistance  $R_{ct}$  evidently increased from 46 to 97  $\Omega$

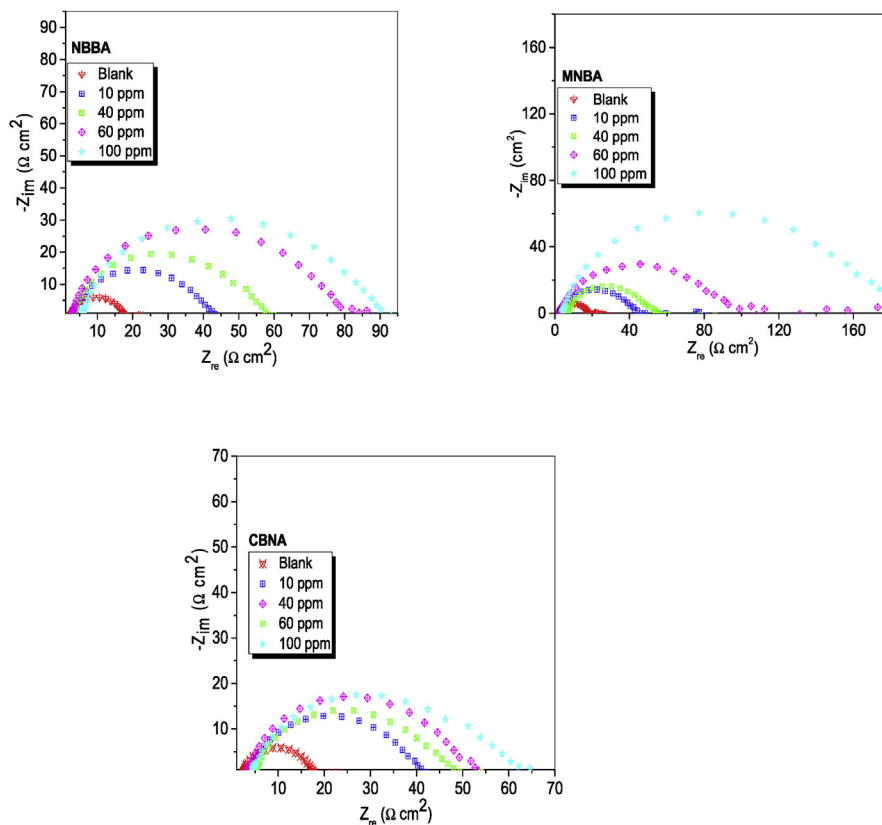


**Fig. 7.** Nyquist plots of the corrosion potential obtained in the absence (blank) and presence of NBBA, MNBA and CBNA at the 10, 40, 60 and 100 ppm concentrations for MS in 1 M HCl.

$\text{cm}^{-2}$ ,  $54\text{--}193 \Omega \text{cm}^{-2}$  and  $45\text{--}74 \Omega \text{cm}^{-2}$  with increase of NBBA, MNBA and CBNA concentration, respectively. Consequently,  $IE_{EIS}$  % was found to increase with the concentration of the three inhibitors. No simple trend could be observed for the CPE constant  $Y_0$  values, however, their reduction in the presence of the studied inhibitors is quite obvious. The choice of CPE ensures adequate description of electrochemical systems involving oxide films, metal/passive film interface and film/electrolyte interface [36]. The phase shift is a gauge of roughness of the surface [21, 36]. The capacitive nature of the CPE in the present investigation has been verified by the values of  $n$  obtained which tend to approach unity. The recorded stability of  $n$  values in the present survey indicates that the MS dissolution is dependent on the charge transfer process [22].

The linear nature of the Bode impedance modulus is more pronounced at high concentrations of the Schiff bases, as shown in Fig. 8. This behaviour enabled us to compute the maximum phase angle ( $-\alpha$ ), and slope ( $-S$ ) at intermediate frequencies which are given in Table 2. The higher slope values obtained for inhibited system especially at maximum concentration indicates that the formed film of the inhibitor species enabled the pseudo-capacitive feature of the electrode interface [21].

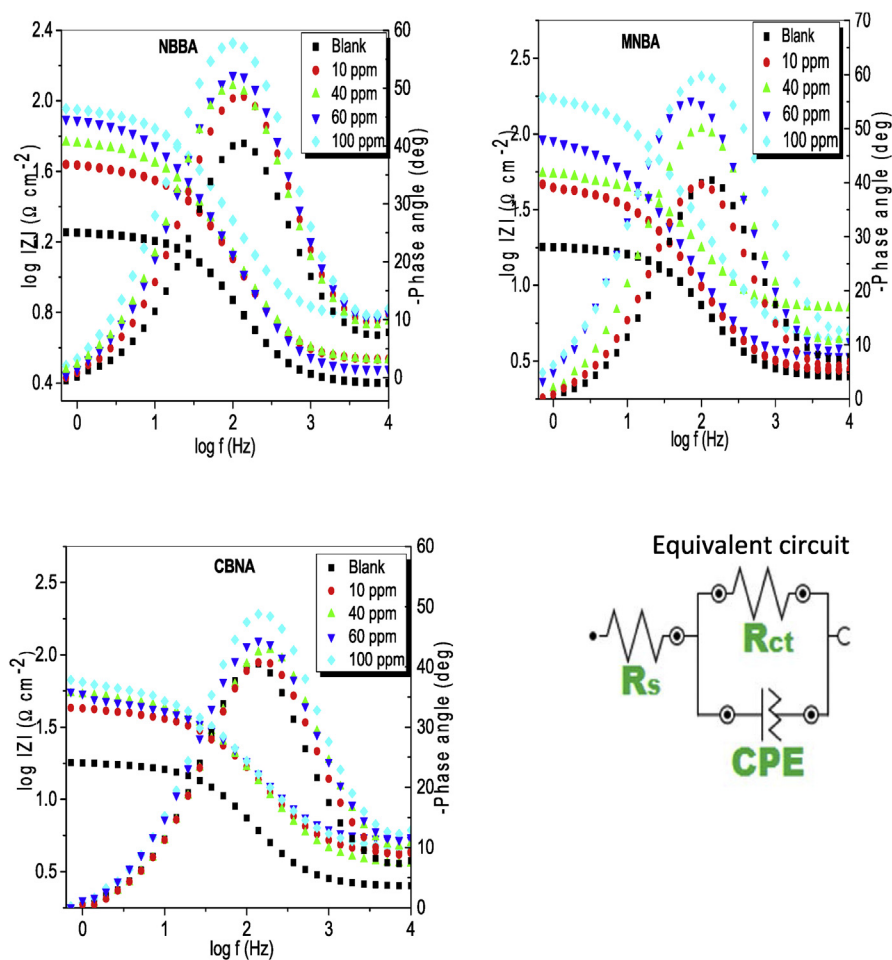


**Fig. 8.** Bode plots for MS in 1 M HCl in the absence (blank) and presence of NBBA, MNBA and CBNA at the following concentrations: 10, 40, 60 and 100 ppm. Equivalent circuit employed in fitting the obtained impedance spectra for MS.

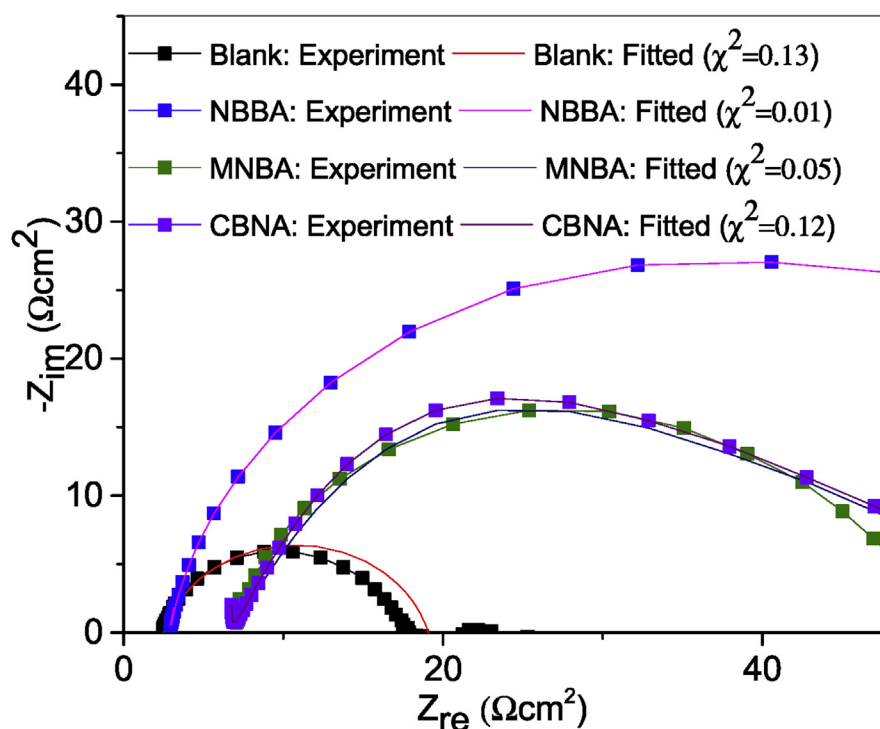
The values of  $IE\%$  obtained for both PDP and EIS measurements corroborate. In addition, the trend in  $IE\%$  of the studied inhibitors suggests that  $MNBA > NBBA > CBNA$ . This trend confers MNBA the most efficient inhibitor for MS corrosion in 1 M hydrochloric acid solution. The overall inhibition efficiencies recorded for this set of inhibitors compare satisfactorily with other structural analogues reported elsewhere [17, 21].

### 3.6. Adsorption isotherm

The extent of inhibitive actions of the studied compounds has been expanded in terms of the adsorption mode of the inhibitor. An efficient organic corrosion inhibitor is expected to adhere onto the metal surface immersed in aqueous solution via a quasi-substitution mode [37, 38, 39, 40, 41]. A correlation between surface coverage

**Table 2.** EIS parameters obtained from EIS plots in the absence and presence of NBBA, MNBA and CBNA at various concentrations for MS in 1 M HCl.

Inhibitor	Conc (ppm)	$R_s$ ( $\Omega \text{ cm}^{-2}$ )	$R_{ct}$ ( $\Omega \text{ cm}^{-2}$ )	$Y_0$ ( $\mu\text{S s}^{-n} \text{ cm}^{-2}$ )	$n$	$\eta\%$	$-\alpha$	$-S$
Blank	—	2.50	17	677	0.84	—	40	0.30
NBBA	10	3.21	46	471	0.81	64	49	0.53
	40	3.21	62	401	0.82	73		
	60	2.82	87	356	0.84	81		
	100	5.57	97	282	0.81	83	50	0.67
MNBA	10	2.51	54	847	0.76	69	50	0.49
	40	6.70	55	500	0.76	69		
	60	3.16	112	548	0.80	85		
	100	4.01	193	203	0.82	91	60	0.58
CBNA	10	3.86	45	505	0.75	62	43	0.44
	40	3.29	56	397	0.78	70		
	60	4.62	60	750	0.68	72		
	100	4.07	74	601	0.71	77	44	0.56

**Fig. 9.** Representative overlays of experimental and fitted data showing Chi-square values.

( $\theta$ ) defined by  $\eta\%/100$  obtained from EIS and the concentrations of inhibitor ( $C_{inh}$ ) were fitted to Langmuir and Frumkin adsorption isotherms. Both isotherms are presented in Fig. 10, and the mathematical forms of the isotherms employed are Equations (8) and (9) [33, 41]:

$$\text{Langmuir: } \frac{C_{inh}}{\theta} = \frac{1}{K_{ads}} + C_{inh} \quad (8)$$

$$\text{Frumkin: } \log \left\{ [C_{inh}] \times \left( \frac{\theta}{1-\theta} \right) \right\} = 2.303 \log K + 2\alpha\theta \quad (9)$$

where  $C_{inh}$  is the concentration of the inhibitor,  $K_{ads}$  is the adsorption equilibrium constant and  $\theta$  is degree of surface coverage of the inhibitor.

Ultimately, the accuracy of the fit was examined using the correlation coefficient ( $R^2$ ) given in Table 3.

As can be observed in Table 3, the  $R^2$  values clearly show that data obtained for the Langmuir isotherms are closer to unity than the Frumkin isotherm. Consequently, the set of inhibitors under study was found to prefer the Langmuir adsorption isotherm. In addition, the values of slope equal to unity obtained for Langmuir isotherm strongly support the idea that, indeed, the group of compounds presented obey the Langmuir adsorption isotherm. In order to ascribe the mechanism of adsorption process to either physisorption or chemisorption, the variation in  $\Delta G_{ads}$  was calculated from Equation (10) [34]:

$$\Delta G_{ads}^{\circ} = -RT \ln(55.5K_{ads}) \quad (10)$$

where  $\Delta G_{ads}^{\circ}$  is the standard free energy of adsorption;  $R$  is the gas constant and  $T$  is the absolute temperature while the value of 55.5 is the concentration of water in solution in  $\text{molL}^{-1}$ . The calculated values of  $K_{ads}$  and  $\Delta G_{ads}^{\circ}$  are recorded in Table 3. The closeness of obtained  $\Delta G_{ads}^{\circ}$  values to  $-40$  suggests a complex mode of adsorption via physisorption and chemisorption of inhibiting species [42].

### 3.7. Scanning electron microscopy (SEM) analysis

SEM micrographs of MS coupons retrieved from 1 M HCl solution after 3 h immersion period in the absence and presence of 100 ppm of NBBA, MNBA and CBNA are presented in Fig. 11. In the absence of inhibitor, the SEM micrograph reveals a seriously degraded surface composed of loosely-held metal oxides. In contrast, the SEM images in the presence of the three inhibitors reveal the absence of corrosion products accompanied by localised pitting on steel surfaces. The micrographs of b–d also reveal cracks due to abrasion during mild steel preparation.

### 3.8. Quantum chemical calculations

The electrochemical data obtained have proven the inhibition efficiency of the compounds, NBBA, MNBA and CBNA for MS corrosion in 1 M aqueous hydrochloric acid. To enhance the quality of the discussion, relevant electronic properties that might have played significant role between the studied inhibitors and MS surface

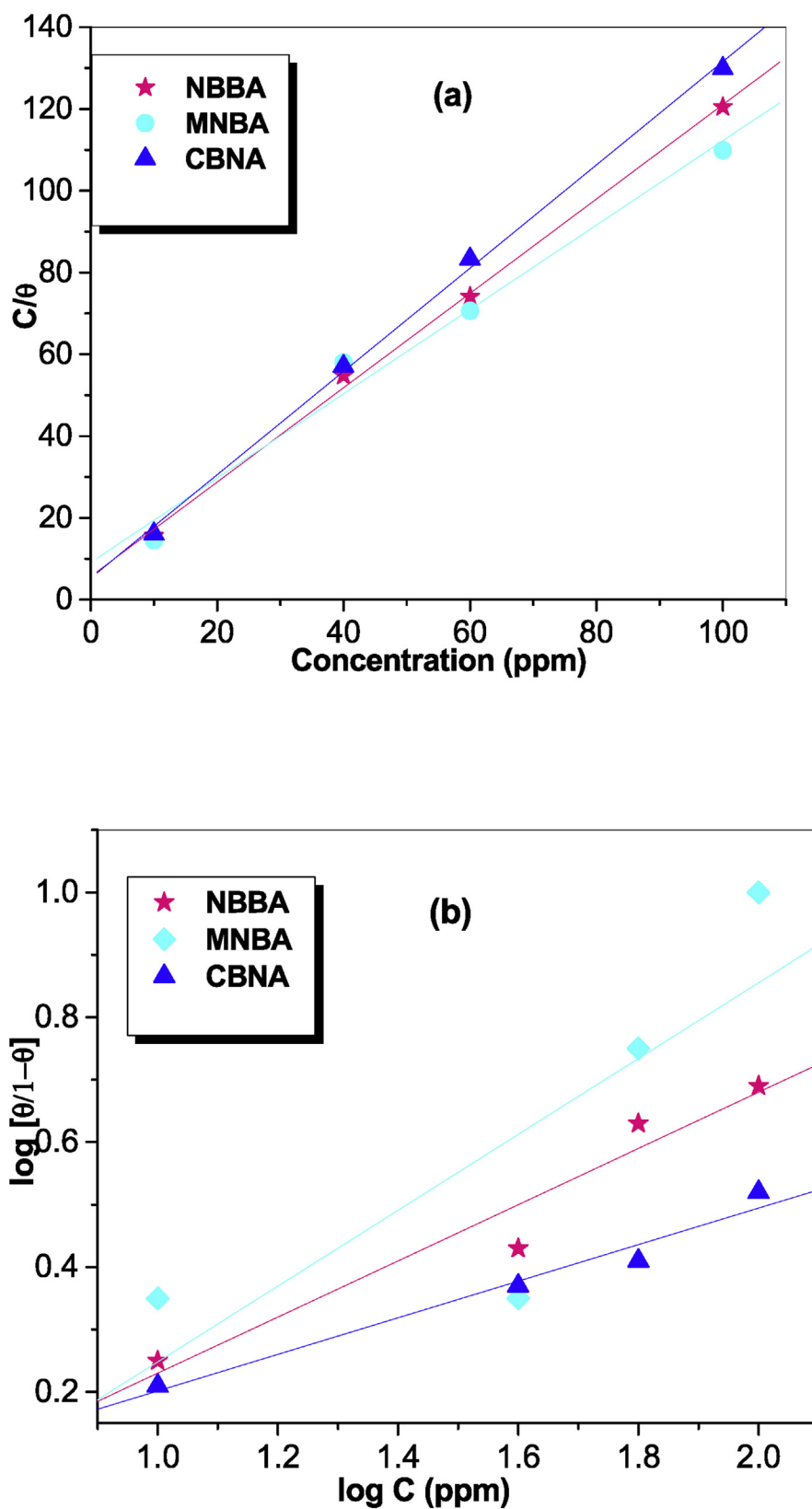
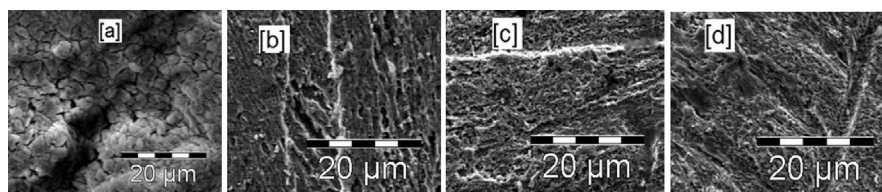


Fig. 10. Plots of (a) Langmuir (b) Frumkin adsorption isotherms for MS in the presence of Schiff bases.

**Table 3.** Adsorption isotherms parameters obtained from EIS data at 303 K.

Inhibitor	Slope	Intercept	R <sup>2</sup>	K <sub>ads</sub>	−ΔG <sub>ads</sub> <sup>o</sup> (kJ/mol)
Langmuir					
NBBA	1.0	5.69	1.0	71253	38.3
MNBA	1.0	9.11	0.99	28023	35.9
CBNA	1.0	5.32	1.0	65936	38.1
Frumkin					
NBBA	0.5	−0.22	0.97	—	—
MNBA	0.6	−0.36	0.82	—	—
CBNA	0.3	−0.09	0.99	—	—

**Fig. 11.** SEM micrographs of MS immersed in 1 M HCl in the absence (a) and presence of 100 ppm of NBBA (b), MNBA (c) and CBNA (d).

were explored using quantum chemical parameters. Fig. 12 presents the optimized structures (in gas phase), HOMO and LUMO electron density isosurfaces of NBBA, MNBA and CBNA. The adsorption of inhibitor species on MS surface is controlled by donor–acceptor mechanisms between inhibitor and the MS. The HOMO electron density isosurface supplies data about the part of the inhibitor molecule from which electrons could easily be donated to the proper vacant orbitals of the metal. The LUMO electron density isosurface, on the other hand, reveals the potential sites that are prone to electron acceptance from the appropriate occupied orbitals of the metal [21, 34, 43, 44]. The HOMO surfaces of the studied Schiff bases are of the  $\pi$ -type and distributed over the entire molecule with little or no contribution from the  $-\text{NO}_2$  group(s). The HOMO is based on the imino nitrogen and the adjoining aromatic rings with significant contribution from the chloride of CBNA.

The LUMO of CBNA shows contributions from phenyl  $\pi^*$ -orbital as well as  $\pi^*$ -orbital of the azomethine moiety. A contribution that is lacking for both NBBA and MNBA where there is no contribution from  $\pi^*$ -orbital of the azomethine moiety and alkyl group.

Additional quantum chemical indices including the  $E_{\text{HOMO}}$ ,  $E_{\text{LUMO}}$ , energy gap ( $\Delta E$ ), dipole moment, absolute hardness ( $\eta$ ), global softness ( $\sigma$ ) and electrophilicity index ( $\omega$ ) were obtained and recorded in Table 4. The parameters were obtained for both gas and water phases using the same level of theory. This was performed in

## Optimised structure

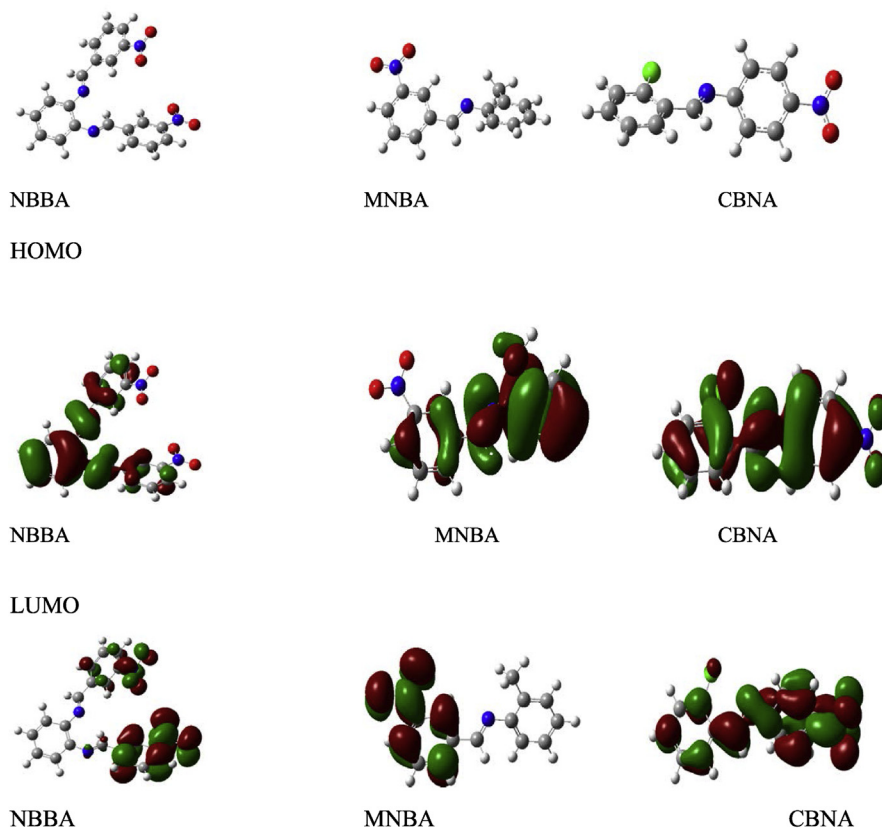


**Fig. 12.** Molecular structures (optimized), HOMO and LUMO electron density distributions of neutral forms of NBBA, MNBA and CBNA.

order to obtain a reliable estimate of electronic properties since corrosion occurs in aqueous medium. These parameters obtained for both phases compare fairly well with each other and suggest that the compounds are efficient inhibitors of MS corrosion in aqueous solution.

A good corrosion inhibitor usually possesses high value of  $E_{\text{HOMO}}$ , and/or low  $E_{\text{LUMO}}$  value, and/or low  $\Delta E$  value, and/or low  $\eta$  value, and/or high  $\sigma$  value. A large  $\omega$  value depicts a better electrophile but a low  $\omega$  value depicts a better nucleophile [21, 45, 46]. From the values of  $E_{\text{HOMO}}$ ,  $E_{\text{LUMO}}$  and electrophilicity index obtained, it could be inferred that NBBA, MNBA and CBNA are efficient inhibitors in their different mode of action. That is, the low  $E_{\text{LUMO}}$  and reasonably high  $\omega$  values of MNBA and CBNA enable them to accept electrons from the vacant d-orbital of MS whereas the high  $E_{\text{HOMO}}$  value of NBBA enables it to donate electrons. Some literature reports allude to the fact that large dipole moment reveals greater inhibition efficiency [47, 48], while a few others infers conversely [49, 50]. Based on the later, the potential trends among the three will follow the order: MNBA > NBBA > CBNA, which suggests that MNBA is the most efficient inhibitor. This trend

**Table 4.** Selected quantum chemical data for the studied Schiff bases.

Inhibitor	$E_{\text{HOMO}}$ (eV)	$E_{\text{LUMO}}$ (eV)	$\Delta E$ (eV)	Dipole moment	$\eta$	$\sigma$	$\omega$
<b>Gas Phase</b>							
NBBA	-6.41	-3.02	3.39	7.38	1.70	0.59	6.55
MNBA	-6.43	-2.95	3.48	5.54	1.74	0.57	6.32
CBNA	-6.91	-2.95	3.96	7.96	1.98	0.51	6.14
<b>Aqueous Phase</b>							
NBBA	-6.28	-3.19	3.09	9.71	1.55	0.65	7.25
MNBA	-6.38	-3.16	3.22	7.54	1.61	0.62	7.07
CBNA	-6.82	-3.14	3.68	10.73	1.84	0.54	6.74
<b>Protonated form</b>							
NBBA	-3.58	-2.91	0.67	8.93	0.34	2.94	15.49
MNBA	-3.97	-3.32	0.65	10.40	0.33	3.03	5.52
CBNA	-4.43	-2.73	1.7	4.37	1.7	0.59	1.05

correlates satisfactorily with the trend in inhibition efficiency obtained from electrochemical test.

It has been established that the heteroatoms of organic species undergo protonation in aggressive aqueous acids which enables them to exist in their cationic form. DFT calculations were therefore performed on the doubly-protonated form of MNBA, NBBA and CBNA in order to provide comprehensive behaviour of inhibitor molecules in 1 M HCl solution. The relevant quantum chemical descriptors recorded for protonated form of MNBA, NBBA and CBNA are presented in Table 4. It can be deduced that the high  $E_{\text{HOMO}}$  of NBBA and the low  $E_{\text{LUMO}}$  values of CBNA qualify them as the preferred candidate for the corrosion inhibition of mild steel in acid solution. In addition, electron donating ability of inhibitors was enhanced in acid solution. The finding corroborates the experimental inhibition efficiency trend and supports the idea that DFT based parameters derived for protonated form of inhibitor molecules are consistent with the trend of DFT indices recorded for their neutral forms.

#### 4. Conclusion

In this work, three Schiff base compounds  $N^1, N^2$ -bis(3-nitrobenzylidene)phenylenediamine (NBBA), 2-methyl- $N$ -(3-nitrobenzylidene)aniline (MNBA) and  $N$ -(2-chlorobenzylidene)-4-nitroaniline (CBNA) were successfully synthesized and characterized by different spectroscopic approaches. The structure of the Schiff bases was further verified using a DFT based calculations. From the studies conducted on the characterized compounds, the following conclusion could be drawn:

1. Both potentiodynamic polarization and electrochemical impedance spectroscopy (PDP and EIS) parameters proved that these Schiff bases are good inhibitors for mild steel corrosion in 1 M HCl solution especially at elevated concentration up to 100 ppm.
2. Potentiodynamic polarization data suggest the Schiff bases are of mixed-type inhibitor while impedance data suggest that their inhibitory activity was based on their adsorption on mild steel surface.
3. The adsorption strength of the three Schiff base compounds was reaffirmed by SEM images with their adsorption mechanisms preferring the Langmuir adsorption isotherm that involves both a physisorption and chemisorption mechanism of inhibiting species.
4. Marked correlation was established between corrosion inhibition efficiency and quantum chemical indices which strongly suggest that the  $\pi^*$ -orbital and position of  $-\text{NO}_2$  had significant influence on the anticorrosion behaviour of the reported Schiff bases.

## Declarations

### Author contribution statement

Elias E. Elemike, Henry U. Nwankwo: Performed the experiments; Analyzed and interpreted the data; Wrote the paper.

Damian C. Onwudiwe: Conceived and designed the experiments; Contributed reagents, materials, analysis tools or data.

### Funding statement

This research did not receive any specific grant from funding agencies in the public, commercial, or not-for-profit sectors.

### Competing interest statement

The authors declare no conflict of interest.

### Additional information

No additional information is available for this paper.

### References

- [1] D.M.C. Maria, R. Da Silva, M.G. Jorge, L.R.S. Ana, C.F.C. Paula, B. Schroder, A.V. Manual, Friedel–crafts alkylation of  $\alpha$ -methylnaphthalene in the presence of ionic liquids, *J. Mol. Catal. Chem.* 224A (2004) 207–212.

- [2] M. Salehi, F. Rahimifar, M. Kubicki, A. Asadi, Structural, spectroscopic, electrochemical and antibacterial studies of some new nickel (II) Schiff base complexes, *Inorg. Chim. Acta* 443 (2016) 28–35.
- [3] S. Shit, S. Sen, S. Mitra, D.L. Hughes, Syntheses, characterization and crystal structures of two square-planar Ni(II) complexes with unsymmetrical tridentate Schiff base ligands and monodentate pseudohalides, *Transit. Met. Chem.* 34 (2009) 269–274.
- [4] S.A. Patil, C.T. Prabhakara, B.M. Halasangi, S.S. Toragalmath, P.S. Badami, DNA cleavage, antibacterial, antifungal and anthelmintic studies of Co(II), Ni(II) and Cu(II) complexes of coumarin Schiff bases: synthesis and spectral approach, *Spectrochim. Acta* 137A (2015) 641–651.
- [5] P. Chakraborty, J. Adhikary, R. Sanyal, A. Khan, K. Manna, S. Dey, E. Zangrando, A. Bauz, A. Frontera, D. Das, Role of ligand backbone of tridentate Schiff-base on complex nuclearity and bio-relevant catalytic activities of zinc(II) complexes: experimental and theoretical investigations, *Inorg. Chim. Acta* 421 (2014) 364–373.
- [6] M. Ghassemzadeh, R. Firouzi, S. Shirkhani, S. Amiri, B. Neumüller, New dinuclear copper(I) metallacycles containing bis-Schiff base ligands fused with two 1,2,4-triazole rings: synthesis, characterization, molecular structures and theoretical calculations, *Polyhedron* 69 (2014) 188–196.
- [7] W. Qin, S. Long, M. Panunzio, S. Biondi, Schiff bases: a short survey on an evergreen chemistry tool, *Molecules* 18 (2013) 12264–12289.
- [8] G. Yadav, J.V. Mani, Green synthesis of Schiff bases by natural acid catalysts, *Int. J. Sci. Res.* 4 (2015) 121–127. ISSN (Online): 2319-7064.
- [9] M. Zbačnik, K. Pičuljan, J. Parlov-Vuković, P. Novak, A. Roodt, Four thermochromic o-hydroxy Schiff bases of  $\alpha$ -aminodiphenylmethane: solution and solid state study, *Crystals* 7 (2017) 25.
- [10] G. Nita, D. Branzea, F. Pop, A. El-Ghayoury, N. Avarvari, Electroactive bisiminopyridine ligands: synthesis and complexation studies, *Crystals* 2 (2012) 338–348.
- [11] R. Ayranci, M. Ak, Synthesis of a novel, fluorescent, electroactive and metal ion sensitive thienylpyrrole derivate, *New J. Chem.* 40 (2016) 8053–8059.
- [12] X.Q. Hao, C.X. Liu, H.P. Li, H. Li, J.F. Gong, M.P. Song, Y.J. Wu, The structures and electrochemistry of Schiff base compounds bearing ferrocene and triazole, *Synth. React. Inorg. Met. Org. Nano Met. Chem.* 39 (2009) 256–260.

- [13] H. Ashassi-Sorkhabia, B. Shaabanib, D. Seifzadeh, Corrosion inhibition of mild steel by some Schiff base compounds in hydrochloric acid, *Appl. Surf. Sci.* 239 (2005) 154–164.
- [14] G. Gunasekaran, L.R. Chauhan, Eco friendly inhibitor for corrosion inhibition of mild steel in phosphoric acid medium, *Electrochim. Acta* 49 (2004) 4387–4395.
- [15] A. Pandey, B. Singh, C. Verma, E.E. Ebenso, Synthesis, characterization and corrosion inhibition potential of two novel Schiff bases on mild steel in acidic medium, *RSC Adv.* 7 (2017) 47148–47163.
- [16] R.K. Gupta, M. Malviya, C. Verma, M.A. Quraishi, Aminoazobenzene and di-aminoazobenzene functionalized graphene oxides as novel class of corrosion inhibitors for mild steel: experimental and DFT studies, *Mater. Chem. Phys.* 198 (2017) 360–373.
- [17] K. Benbouguerra, S. Chafaa, N. Chafai, M. Mehri, O. Moumeni, A. Hellal, Synthesis, spectroscopic characterization and a comparative study of the corrosion inhibitive efficiency of an  $\alpha$ -aminophosphonate and Schiff base derivatives: experimental and theoretical investigations, *J. Mol. Struct.* 1157 (2018) 165–176.
- [18] A.A. Farag, M.A. Hegazy, Synergistic inhibition effect of potassium iodide and novel Schiff bases on X65 steel corrosion in 0.5 M H<sub>2</sub>SO<sub>4</sub>, *Corros. Sci.* 74 (2013) 168–177.
- [19] N. Chafai, S. Chafaa, K. Benbouguerra, D. Daoud, A. Hellal, M. Mehri, Synthesis, characterization and the inhibition activity of a new  $\alpha$ -aminophosphonic derivative on the corrosion of XC48 carbon steel in 0.5 M H<sub>2</sub>SO<sub>4</sub>: experimental and theoretical studies, *J. Taiwan Inst. Chem. Eng.* 70 (2017) 331–344.
- [20] E.E. Elemike, H.U. Nwankwo, D.C. Onwudiwe, E.C. Hosten, Synthesis, crystal structures, quantum chemical studies and corrosion inhibition potentials of 4-(((4-ethylphenyl)imino)methyl)phenol and (E)-4-((naphthalen-2-ylimino)methyl) phenol Schiff bases, *J. Mol. Struct.* 1147 (2017) 252–265.
- [21] E.E. Elemike, D.C. Onwudiwe, H.U. Nwankwo, E.C. Hosten, Synthesis, crystal structure, electrochemical and anti-corrosion studies of Schiff base derived from o-toluidine and o-chlorobenzaldehyde, *J. Mol. Struct.* 1136 (2017) 253–262.
- [22] E.E. Elemike, H.U. Nwankwo, D.C. Onwudiwe, E.C. Hosten, Synthesis, structures, spectral properties and DFT quantum chemical calculations of (E)-4-(((4-propylphenyl)imino)methyl)phenol and (E)-4-((2-tolylimino)

- methyl)phenol; their corrosion inhibition studies of mild steel in aqueous HCl, *J. Mol. Struct.* 1141 (2017) 12–22.
- [23] C. Lee, W.T. Yang, R.G. Parr, Development of the Colle-Salvetti correlation-energy formula into a functional of the electron density, *Phys. Rev. B* 37 (1988) 785–789.
- [24] A.D. Becke, Density-functional thermochemistry III: the role of exact exchange, *J. Chem. Phys.* 98 (1993) 5648–5652.
- [25] M.J. Frisch, G.W. Trucks, H.B. Schlegel, G.E. Scuseria, M.A. Robb, J.R. Cheeseman, J.A. Montgomery, T. Vreven, K.N. Kudin, J.C. Burant, J.M. Millam, S.S. Iyengar, J. Tomasi, V. Barone, B. Mennucci, M. Cossi, G. Scalmani, N. Rega, G.A. Petersson, H. Nakatsuji, M. Hada, M. Ehara, K. Toyota, R. Fukuda, J. Hasegawa, M. Ishida, T. Nakajima, Y. Honda, O. Kitao, H. Nakai, M. Klene, X. Li, J.E. Knox, H.P. Hratchian, J.B. Cross, V. Bakken, C. Adamo, J. Jaramillo, R. Gomperts, R.E. Stratmann, O. Yazyev, A.J. Austin, R. Cammi, C. Pomelli, J.W. Ochterski, P.Y. Ayala, K. Morokuma, G.A. Voth, P. Salvador, J.J. Dannenberg, V.G. Zakrzewski, S. Dapprich, A.D. Daniels, M.C. Strain, O. Farkas, D.K. Malick, A.D. Rabuck, K. Raghavachari, J.B. Foresman, J.V. Ortiz, Q. Cui, A.G. Baboul, S. Clifford, J. Cioslowski, B.B. Stefanov, G. Liu, A. Liashenko, P. Piskorz, I. Komaromi, R.L. Martin, D.J. Fox, T. Keith, M.A. Al-Laham, C.Y. Peng, A. Nanayakkara, M. Challacombe, P.M.W. Gill, B. Johnson, W. Chen, M.W. Wong, C. Gonzalez, J.A. Pople, Gaussian 03W, Revision E. 01, Gaussian Inc, Wallingford, CT, 2004.
- [26] N. Boussalah, S. Ghalem, S. El Kadiri, B. Hammouti, R. Touzani, Theoretical study of the corrosion inhibition of some bipyrazolic derivatives: a conceptual DFT investigation, *Res. Chem. Intermed.* 34 (2012) 2009–2023.
- [27] E.G. Demissie, S.B. Kassa, G.W. Woyessa, Quantum chemical study on corrosion inhibition efficiency of 4-amino-5-mercapto-1,2,4-triazole derivatives for copper in HCl solution, *Int. J. Sci. Eng. Res.* 5 (2014) 304–312. ISSN 2229-5518.
- [28] H. Elmsellem, H. Nacer, F. Halaimia, A. Aouniti, I. Lakehal, A. Chetouani, S.S. Al-Deyab, I. Warad, R. Touzani, B. Hammouti, Anti-corrosive properties and quantum chemical study of (E)-4-methoxy-N-(methoxybenzylidene)aniline and (E)-N-(4-methoxybenzylidene)-4-nitroaniline coating on mild steel in molar hydrochloric, *Int. J. Electrochem. Sci.* 9 (2014) 5328–5351.
- [29] H.U. Nwankwo, L.O. Olasunkanmi, E.E. Ebenso, Experimental, quantum chemical and molecular dynamic simulations studies on the corrosion inhibition of mild steel by some carbazole derivatives, *Sci. Rep.* 7 (2017) 1–18.

- [30] A. Mboniyirivuze, B. Mwakikunga, S.M. Dhlamini, M. Maaza, Fourier transform infrared spectroscopy for sepia melanin, *Phys. Mater. Chem.* 3 (2015) 25–29.
- [31] W. Kemp, *Organic Spectroscopy*, vol. 71, Macmillan Press, London, 1991.
- [32] M. Behpour, S.M. Ghoreishi, N. Soltani, M. Salavati-Niasari, M. Hamadianian, A. Gandomi, Electrochemical and theoretical investigation on the corrosion inhibition of mild steel by thiosalicylaldehyde derivatives in hydrochloric acid solution, *Corros. Sci.* 50 (2008) 2172–2181.
- [33] H.U. Nwankwo, L.O. Olasunkanmi, E.E. Ebenso, Electrochemical and computational studies of some carbazole derivatives as inhibitors of mild steel corrosion in abiotic and biotic environments, *J. Bio Tribo Corros.* 4 (2018) 1–17.
- [34] H.U. Nwankwo, C.N. Ateba, L.O. Olasunkanmi, S. Abolanle, A.S. Adekunle, D.A. Isabirye, D.C. Onwudiwe, E.E. Ebenso, Synthesis, characterization, antimicrobial studies and corrosion inhibition potential of 1, 8-dimethyl-1, 3, 6, 8, 10, 13-hexaazacyclotetradecane: experimental and quantum chemical studies, *Materials* 9 (2016) 1–19.
- [35] D.K. Yadav, M.A. Quraishi, B. Maiti, Inhibition effect of some benzylidenes on mild steel in 1 M HCl: an experimental and theoretical correlation, *Corros. Sci.* 55 (2012) 254–266.
- [36] M. Bojinov, G. Fabricius, T. Laitinen, K. Mäkeliä, T. Saario, G. Sundholm, Coupling between ionic defect structure and electronic conduction in passive films on iron, chromium and iron-chromium alloys, *Electrochim. Acta* 45 (2000) 2029–2048.
- [37] A. Ostovari, S.M. Hoseinieh, M. Peikari, S.R. Shadizadeh, S.J. Hashemi, Corrosion inhibition of mild steel in 1 M HCl solution by henna extract: a comparative study of the inhibition by henna and its constituents (Lawsone, Gallic acid,  $\alpha$ -D-Glucose and Tannic acid), *Corros. Sci.* 51 (2009) 1935–1949.
- [38] L.R. Chauhan, G. Gunasekaran, Corrosion inhibition of mild steel by plant extract in dilute HCl medium, *Corros. Sci.* 49 (2007) 1143–1161.
- [39] H. Ashassi-Sorkhabi, M.R. Majidi, K. Seyyedi, Investigation of inhibition effect of some amino acids against steel corrosion in HCl solution, *Appl. Surf. Sci.* 225 (2004) 176–185.
- [40] L.A. Nnanna, O.C. Nwadiuko, N.D. Ekekwe, C.F. Ukpabi, S.C. Udensi, K.B. Okeoma, B.N. Onwuagba, I.M. Mejeha, Adsorption and inhibitive

- properties of leaf extract of *Newbouldia leavis* as a green inhibitor for aluminium alloy in  $\text{H}_2\text{SO}_4$ , *Am. J. Mater. Sci.* 1 (2011) 143–148.
- [41] C.A. Başar, Applicability of the various adsorption models of three dyes adsorption onto activated carbon prepared waste apricot, *J. Hazard. Mater. B* 135 (2006) 232–241.
- [42] S.K. Saha, A. Dutta, P. Ghosh, D. Sukul, P. Banerjee, Novel Schiff-base molecules as efficient corrosion inhibitors for mild steel surface in 1 M HCl medium: experimental and theoretical approach, *Phys. Chem. Chem. Phys.* 18 (2016) 17898–17911.
- [43] F. Bentiss, B. Mernari, M. Traisnel, H. Vezin, M. Lagrenée, On the relationship between corrosion inhibiting effect and molecular structure of 2,5-bis(*n*-pyridyl)-1,3,4-thiadiazole derivatives in acidic media: Ac impedance and DFT studies, *Corros. Sci.* 53 (2011) 487–495.
- [44] K. Babić-Samardžija, K.F. Khaled, N. Hackerman, Investigation of the inhibiting action of O-, S- and N-dithiocarbamate(1,4,8,11-tetraazacyclotetradecane) cobalt(III) complexes on the corrosion of iron in  $\text{HClO}_4$  acid, *Appl. Surf. Sci.* 240 (2005) 327–340.
- [45] H. Wang, X. Wang, H. Wang, L. Wang, A. Liu, DFT study of new bipyrazole derivatives and their potential activity as corrosion inhibitors, *J. Mol. Model.* 13 (2007) 147–153.
- [46] P. Udhayakala, T.V. Rajendiran, A theoretical evaluation on benzothiazole derivatives as corrosion inhibitors on mild steel, *Der Pharma Chem.* 7 (2015) 92–99. ISSN 0975-413X.
- [47] H. Tanak, A. Ağar, M. Yavuz, Experimental and quantum chemical calculation studies on 2-[(4-Fluorophenylimino) methyl]-3, 5-dimethoxyphenol, *J. Mol. Model.* 16 (2010) 577–587.
- [48] R. Hasanov, M. Sadikoğlu, S. Bilgiç, Electrochemical and quantum chemical studies of some Schiff bases on the corrosion of steel in  $\text{H}_2\text{SO}_4$  solution, *Appl. Surf. Sci.* 253 (2007) 3913–3921.
- [49] G. Gece, The use of quantum chemical methods in corrosion inhibitor studies, *Corros. Sci.* 50 (2008) 2981–2992.
- [50] J. Saranya, P. Sounthari, K. Parameswari, S. Chitra, Acenaphtho[1,2-*b*]quinoxaline and acenaphtho[1,2-*b*]pyrazine as corrosion inhibitors for mild steel in acid medium, *Measurement* 77 (2016) 175–186.